OLD DOMINION UNIVERSITY RESEARCH FOUNDATION

DEPARTMENT OF PHYSICS AND GEOPHYSICAL SCIENCES
SCHOOL OF SCIENCES AND HEALTH PROFESSIONS
OLD DOMINION UNIVERSITY
NORFOLK, VIRGINIA

Technical Report PGSTR-PH76-28

A STUDY OF SATELLITE REMOTE MEASUREMENTS OF STRATOSPHERIC AEROSOL AND GAS PARAMETERS USING THE SOLAR OCCULTATION TECHNIQUE

By

William P. Chu

Final Report

Prepared for the
National Aeronautics and Space Administration
Langley Research Center
Hampton, Virginia

Under
Grant NSG 1108
September 1974 - January 1976

April 1976

DEPARTMENT OF PHYSICS AND GEOPHYSICAL SCIENCES
SCHOOL OF SCIENCES AND HEALTH PROFESSIONS
OLD DOMINION UNIVERSITY
NORFOLK, VIRGINIA

Technical Report PGSTR-PH76-28

A STUDY OF SATELLITE REMOTE MEASUREMENTS OF STRATOSPHERIC AEROSOL AND GAS PARAMETERS USING THE SOLAR OCCULTATION TECHNIQUE

By

William P. Chu

Final Report

Prepared for the
National Aeronautics and Space Administration
Langley Research Center
Hampton, Virginia 23665

Under
Grant NSG 1108
September 1974 - January 1976
Michael P. McCormick, Technical Monitor
Instrument Research Division

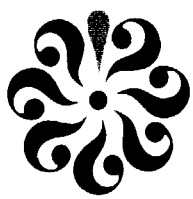

Submitted by the
Old Dominion University Research Foundation
Norfolk, Virginia 23508

April 1976

A STUDY OF SATELLITE REMOTE MEASUREMENTS OF STRATOSPHERIC AEROSOL AND GAS PARAMETERS USING THE SOLAR OCCULTATION TECHNIQUE

By

William P. Chu[1]

SUMMARY

This report contains results of research investigations performed during the period from September 1974 to December 1975 under grant NSG 1108. Satellite remote measurements of stratospheric aerosol and ozone profiles using the solar occultation approach have been analyzed based on the known properties of the atmospheric parameters. Atmospheric refraction effects which are important in this experiment have been determined analytically. Different inversion techniques have been developed based on inverting simulated irradiance data. It is shown that aerosol and ozone profiles in the stratosphere can be inverted from the irradiance measurements to an accuracy of better than 10 percent.

---

[1] Research Assistant Professor in Physics, School of Sciences and Health Professions, Old Dominion University, Norfolk, VA 23508.

INTRODUCTION

The purpose of the work performed under this grant was to analyze the methods for determining stratospheric aerosol and ozone profiles from satellite measurements of atmospheric extinctions during solar occultation. Solar occultation experiments have been carried out successfully by Pepin (ref. 1) using a high altitude balloon. With an orbiting satellite as the observation platform, this technique can be used for remotely monitoring stratospheric constituents with global coverage.

In this report we describe the geometry of the experiment and derive the basic equation relating the solar radiance to the measured irradiance. Atmospheric refraction effects which play an important role in determining the geometry of the experiment are analyzed.

The inversion problems are examined and different inversion schemes have been developed. The sensitivity of the different inversion techniques to experimental errors has been analyzed.

DESCRIPTION OF THE EXPERIMENT

In the solar occultation experiment, multi-wavelength measurements of the attenuation of solar radiation along a tangent path through the atmosphere are made on board the spacecraft. The basic geometry of the experiment is illustrated in figure 1. As the spacecraft emerges from the Earth's shadow, the radiometer aboard the spacecraft will point to the Sun, measuring solar radiation at several preselected wavelength bands. As the spacecraft continues in its orbit, the line of sight from the spacecraft to the Sun will scan the Earth's atmosphere at different tangent altitudes, resulting in a measurement of attenuated solar radiation at different atmospheric heights. Only two vertical profiles of the atmosphere can be obtained for each orbit corresponding to spacecraft sunset and sunrise events.

Assuming the Earth's atmosphere is divided into several concentric, homogeneous layers of equal thickness, then the path length along the line of sight at a given tangent height is much greater for the tangent layer than for any other layers. This implies that

the major attenuation will take place within this particular tangent layer, and can result in a very high vertical resolution measurement of atmospheric constituents.

EXTINCTION MODEL OF THE STRATOSPHERE

In the wavelength range from 0.3 to 1.0 micron, stratospheric attenuations are predominantly caused by aerosol, ozone, and air molecules (Rayleigh component) with minor contributions from NO_2, water vapor and O_2 molecules. The peak of the aerosol distribution generally occurs at an altitude of 18 km while the peak of the ozone profile occurs at 23 km. Models of the stratospheric extinction versus wavelength profiles can be constructed from different vertical distributions of aerosol and ozone. Figure 2 shows an extinction coefficient model as a function of wavelength at the aerosol peak altitude of 18 km. Figure 3 shows the extinction model at the ozone peak altitude of 23 km. The aerosol vertical distribution used in generating these plots was based on Fenn's (ref. 2) moderate volcanic model, while the ozone profile was based on Elterman's model (ref. 3). The aerosol extinction as a function of wavelength can be calculated from the particle size distribution, total density, and index of refraction. Figure 4 shows the same extinction model at an altitude of 30 km. NO_2 extinction which was computed from recent measurements (ref. 4) shows some contribution to the total extinction at high altitude.

BASIC EQUATIONS

The equations relating the observed irradiance to the atmospheric extinction profiles can be derived by considering the geometry as shown in figure 1. For a radiometer situated on a satellite with orbital velocity vector $\vec{v}$, a single ray originating from the Sun with intensity I_s, after propagating through the atmosphere with tangent height h_T will reach the radiometer making an angle θ with respect to the vector $\vec{v}$. The intensity reaching the radiometer $I(\theta)$ will be given by

$$I(\theta) = \tau_\lambda(h_T) I_s \tag{1}$$

where $\tau_\lambda(h_T)$ is the transmission function of the atmosphere at wavelength λ and is given by the Lambert-Beer Law as

$$\tau_\lambda(h_T) = \exp\left\{-2\int_{h_T}^{\infty} \beta_\lambda(h)\, dP_\lambda(h)\right\} \tag{2}$$

$\beta_\lambda(h)$ is the total extinction profile of the atmosphere at wavelength λ including contributions from aerosol, Rayleigh component, and other gases. $P_\lambda(h)$ is the ray path length at wavelength λ.

Assuming the atmosphere is spherically stratified and spherically symmetric, then each sunray making a view angle of θ with respect to the vector $\vec{v}$ at the radiometer will define a tangent height $h_T(\theta)$. The solar radiance distribution $N_\lambda(\theta)$ at the entrance window to the radiometer will be given by the following equation

$$N_\lambda(\theta,t) = S_\lambda(\theta,t)\ \ \tau_\lambda\left[h_T(\theta)\right] \tag{3}$$

$S_\lambda(\theta,t)$ is the refracted but unattenuated solar radiance profile at time t which is determined by the solar limb darkening profile at wavelength λ. The effects due to atmospheric refraction will be discussed in more detail in the next section. Both N_λ and S_λ are in units of Watts/cm^2-Ω. The irradiance received by the radiometer will then by given by

$$H_\lambda(\theta_i) = \int F_\lambda(\theta,\theta_i)\ S_\lambda(\theta,t_i)\ \ \tau_\lambda\left[h_T(\theta)\right]\, d\Omega \tag{4}$$

where $F_\lambda(\theta,\theta_i)$ is the radiometer's field of view (FOV) function centered at view angle θ_i, and $H_\lambda(\theta)$ is the irradiance received by the radiometer at time t_i when the FOV is pointing at view angle θ_i.

Equation (4) is the desired result relating the observed irradiance to the source function S_λ and the transmission function of the

atmosphere τ_λ. The transmission function τ_λ is independent of the spacecraft geometry and is defined solely by the extinction profile $\beta(h)$ of the atmosphere through equation (2).

ATMOSPHERIC REFRACTION

Atmospheric refraction is an important factor to be considered in the solar occultation experiment. The effects can be dramatic, especially in the lower stratospheric layers where bending of sunrays is pronounced. In the following section we will describe a ray trace method to calculate atmospheric refraction effects.

1. Ray Trace Analysis

Consider a spherically symmetric atmosphere, the equation governing a ray path is (ref. 5)

$$n(r)\, r \sin \phi = \text{constant} \tag{5}$$

where $n(r)$ is the refractive index at position r with respect to the Earth's center, ϕ is the angle between the position vector and the ray tangent vector at r. Referring to figure 5, we assume the spacecraft is situated at point P_o at a distance of r_o from the Earth's center. Defining Cartesian x-y axes at the Earth's center, we start a ray propagating at an angle θ_o from the x-axis. We have from equation (5)

$$n(r_o)\, r_o \sin \phi_o = C_o \tag{6}$$

where $r_o = (x_o^2 + y_o^2)^{1/2}$, and ϕ_o is related to θ_o as

$$\phi_o = \cos^{-1}\left(\frac{\vec{r}_o \cdot \hat{e}_x}{r_o}\right) - \theta_o \tag{7}$$

where $\hat{e}_x$ is the unit vector along the x-axis. We now trace a small segment of ray with length Δs and arrive at point P_1 at a distance r_1 from the Earth's center where

$$r_1 = \left\{ (x_o + \Delta s \cos \theta_o)^2 + (y_o + \Delta s \sin \theta_o)^2 \right\}^{1/2} \quad (8)$$

The ray direction at P_1 can now be computed from equation (5) to be

$$\phi_1 = \sin^{-1} \left(\frac{C_o}{n(r_1) r_1} \right) \quad (9)$$

and the new angle θ_1 is given by

$$\theta_1 = \cos^{-1} \left(\frac{\vec{r}_1 \cdot \hat{e}_x}{r_1} \right) - \phi_1 \quad (10)$$

We can continue this process until the ray passes through the atmosphere and determine the final angle θ_f. Moreover, the tangent height of this ray can be determined from the r value when $\phi = \pi/2$.

The above procedure can be done for a large number of rays with different initial ray angles. We then generate a table of three parameters; the initial ray angle θ_o, the final ray angle θ_f, and the corresponding ray tangent height h_T. The relationship between these three parameters will completely describe the refraction effects.

2. Ray Trace Results

The ray trace method has been applied to atmospheres with different temperature and pressure distributions. The refractive index $n(r)$ of air depends on its density as (ref. 6)

$$n(r) = 1 + A_\lambda \rho(r) \quad (11)$$

where $\rho(r)$ is the density of air determined by the temperature and pressure distributions, and A_λ is a constant which differs for different wavelengths.

Figure 6 shows results from the ray trace calculation for a satellite at orbital altitude of 600 km viewing the Sun. An orbital

period of 90 minutes was used to compute the time variation of the Sun shape for a sunset event. The atmosphere used was the standard 1962 mid-latitude atmospheric profile. The top and bottom of the solar disk as observed on the image plane of the radiometer are shown as the satellite heading toward the Earth's shadow. It is obvious that the Sun images are continuously being demagnified.

Figure 7 shows the computed Sun images as observed on the spacecraft for a sunset event. The vertical dimension of the Sun images can be demagnified by a factor of four as the apparent height of the Sun is at 10 km altitude. Computations of the refracted but unattenuated solar radiance profiles $S_\lambda(\theta,t)$ can now be performed based on the refraction calculation as derived above.

INVERSION TECHNIQUES

In the solar occultation experiment, the radiometer aboard the spacecraft will measure solar irradiance as the line of sight of the instrument scans across the vertical tangent height of the atmosphere. Equation (4) will reduce to a set of m equations describing the irradiance measured at m different view angles θ_i.

$$H_\lambda(\theta_i) = \int F_\lambda(\theta,\theta_i)\, S_\lambda(\theta,t)\, \exp\left\{-2\int_{h_T(\theta)}^{\infty} \beta_\lambda(h)\,dP(h)\right\} d\Omega \qquad (12)$$

$$i = 1, 2, \ldots m$$

Given a set of measurements $H_\lambda(\theta_i)$, equation (12) is nonlinear in the unknown $\beta_\lambda(h)$. The techniques used for the solution of equation (12) will depend on the functional form of the instrument FOV function $F_\lambda(\theta,\theta_i)$. We will discuss this in the following two special cases of interest.

1. Case 1: Radiometer with Small FOV

If the vertical resolution of the radiometer's FOV is small compared to the vertical structure of the atmosphere which is of interest

we can assume the transmission function $\tau_\lambda[h_T(\theta)]$ to be constant for each irradiance measurement. Defining an effective optical depth g_i, we have from equation (2)

$$g_i = 2\int_{h_T(\theta_i)}^{\infty} \beta_\lambda(h)\, dP(h) \tag{13}$$

where g_i is related to the measurement by

$$g_i = \ln\left\{\int F_\lambda(\theta,\theta_i)\, S_\lambda(\theta,t_i)d\Omega/H_\lambda(\theta_i)\right\} \tag{14}$$

Equation (13) is a Fredholm integral equation of the first kind. The integral can be approximated with n discrete atmospheric layers with equal thickness, and the equations can be replaced by the following linear system of equations

$$g_i = \sum_{j=i} P_{ij}\, \beta_j \qquad i = 1, 2, \ldots m \tag{15}$$

where β_j is the total extinction coefficient in the jth atmospheric layer, and P_{ij} is the ray path length in the jth layer with tangent height at the ith layer. Equation (15) can be abbreviated into a matrix form

$$g = P\beta \tag{16}$$

Equation (16) can be solved directly for β either exactly when $n = m$ or in the least-square sense when $n < m$,

$$\beta = P^{-1}g \qquad n = m \tag{17}$$

$$\beta = (P^T P)^{-1}P^T g \qquad n < m \tag{18}$$

where P^{-1} is the inverse of P, and P^T is the transpose of P.

The direct inversion schemes are generally unstable due to the presence of noise term associated with the measurements g_i. In order to suppress unwanted oscillations in the solutions, the smoothing method developed by Twomey (ref. 7) and Phillips (ref. 8) can be used. The smoothing method imposes certain constraint on the solutions, and the most widely used constraint has been the minimization of the second-difference expression $\sum_i (\beta_{i-1} - 2\beta_i + \beta_{i+1})^2$. The resulting solutions are given by the following form

$$\beta = (P^T P + \gamma H)^{-1} P^T g \tag{19}$$

where H is the second-difference constraint matrix and γ is the smoothing parameter whose magnitude is dependent on the noise level in the measurements.

2. Case 2: Radiometer with Large FOV

This case generally does not arise unless the radiometer is measuring the irradiance from the whole Sun. The inversion of equation (12) in this case generally begins by linearizing the integral equations in some ways. One form of linearization uses an expansion of the solution $\beta_\lambda(h)$ around some initial guessed profile $\beta^o_\lambda(h)$

$$\beta_\lambda(h) = \beta^o_\lambda(h) + \Delta\beta_\lambda(h) \tag{20}$$

Assuming that

$$2\int_{h_T}^{\infty} \Delta\beta_\lambda(h)dP(h) << 1 \tag{21}$$

we can reduce the transmission function to the following form,

$$\tau_\lambda[h_T(\theta)] = \tau^o_\lambda[h_T(\theta)] \left\{1 - 2\int_{h_T}^{\infty} \Delta\beta_\lambda(h)dP(h)\right\} \tag{22}$$

where

$$\tau_\lambda^o\ [h_T(\theta)] = \exp\left\{-2\int_{h_T}^{\infty} \beta_\lambda^o\ (h)dP(h)\right\} \tag{23}$$

Substituting equation (22) into equation (12), and assuming $F_\lambda(\theta,\theta_i) = 1$, we obtain

$$H_\lambda(\theta_i) = H_\lambda^o(\theta_i) + \int S_\lambda(\theta,t_i)\tau_\lambda^o\ [h_T(\theta)] \times \left\{-2\int_{h_T}^{\infty} \Delta\beta_\lambda(h)dP(h)\right\}\ d\Omega \tag{24}$$

where

$$H_\lambda^o(\theta_i) = \int S_\lambda(\theta,t_i)\tau_\lambda^o\ [h_T(\theta)]d\Omega \tag{25}$$

The double integral in equation (24) can be approximated by the following system of equations

$$\Delta H_i = \sum_{j=1}^{n}\ \sum_{k=j}^{n}\ S_{ij}\ \tau_j^o\ P_{jk}\ \Delta\beta_k \tag{26}$$

where $\Delta H_i = H_\lambda(\theta_i) - H_\lambda^o(\theta_i)$, and S_{ij} is the solar irradiance contribution in the ith measurement from the jth atmospheric layer. Defining $K_{ik} = \sum_j S_{ij}\ \tau_j^o\ P_{jk}$, equation (26) then becomes

$$\Delta H_i = \sum_{k=1}^{n} K_{ik}\ \Delta\beta_k \tag{27}$$

or in abbreviated matrix form

$$\Delta H = K\Delta\beta \tag{28}$$

Equation (28) is identical in form to equation (16) so that the previously discussed methods of solution can be applied here. However, the initial guessed profile $\beta_\lambda^o(h)$ in this case could be quite poor. A method of solution in which the initial guessed profile is continuously updated can be done with the iterative scheme. One form of the iterative scheme which is based on Twomey's work (refs. 7, 9) is

$$\beta^{\ell+1} = \beta^\ell + K^T(KK^T + \gamma)^{-1}\ [H_m - H^\ell] \tag{29}$$

where β^ℓ is the ℓth order inverted β profile, H_m is the measured irradiance, H^ℓ is the ℓth order computed irradiance, and γ is the ratio of noise variance to signal variance. The iteration will stop when the difference between the computed irradiance and the measurements are within the instrument noise level. Another form of the iterative scheme which was developed by Conrath and Revah (ref. 9) and Smith (ref. 10) is

$$\beta^{\ell+1} = \beta^\ell + G^{-1}\ K^T(H_m - H^\ell) \tag{30}$$

where G is a diagonal matrix with elements $G_{jj} = 1/\sum_i K_{ij}$. A comparison of the two iterative schemes in satellite remote temperature probing has been discussed by Conrath and Revah (ref. 9).

SENSITIVITY ANALYSIS

The sensitivity of the inversion techniques to various experimental errors has been analyzed based on the inversion of different computer simulated irradiance profiles. These analyses have been performed in order to establish the accuracy of the inversion approaches and the accuracy requirement for different instrumentation design parameters.

The first step in generating the expected irradiance profiles is to compute the atmospheric transmission function $\tau_\lambda(h)$ at several preselected wavelengths. We have chosen wavelengths at 0.38, 0.45, 0.6, and 1.0 μm to coincide with the spectral channel locations for the Stratospheric Aerosol and Gas Experiment (SAGE). The 0.6 micron channel is the ozone channel while the other three are primarily aerosol channels. Figure 8 shows the calculated transmission versus altitude profiles for the four wavelengths based on Elterman's aerosol and ozone models (ref. 3). These calculations have included atmospheric refraction effects based on the standard 1962 mid-latitude atmospheric temperature and pressure profiles.

To incorporate the spacecraft geometry in generating the irradiance profiles, we consider a radiometer with field of view of 30 arc seconds, situated on a satellite at orbital altitude of 600 km. The radiometer is assumed to point at the solar disk at 10 arc minutes from the vertical top edge during the complete sunrise or sunset event.

The inversion of these irradiance profiles was then performed by introducing experimental errors of various origins and magnitudes to the irradiance profiles. There are two types of errors which will directly affect the inversion results. The first type of error is noise associated with the desired signals. This random noise has both optical and electrical origins. The optical contributions are dominated by irradiance detected from outside the instrumental spectral bandwidth and outside the instantaneous field of view. The electrical contributions are the usual quantization error in the A to D converter and noise in the electronics. The second type of error is associated with the pointing system. Since the radiometer's pointing can be controlled by a servo mechanism in maintaining a fixed location on the solar image, a slight fluctuation in the servo system can produce uncertainty in the instantaneous viewing direction and result in tangent-height error. These tangent-height errors when considering different amounts of attenuation at different tangent altitudes, plus the solar limb darkening profiles, will generate irradiance errors.

The two types of errors mentioned above in different magnitudes were added to the expected irradiance profiles and inversions were performed to determine their effects. The atmosphere was divided

into homogeneous layers of 1-km thickness with inversion performed for each layer. Figures 9 through 12 show the direct inversion results based on equation (17) for the four channels simulated irradiance profiles. An instrumental noise level of 1 percent of reading and pointing errors of 3 arc seconds (one sigma) have been included. The results indicated that aerosol extinction profiles from the three aerosol channels can be inverted with an accuracy of about 10 percent from 10 to 30 km altitude. Similary, ozone extinction profiles can be extracted to about 10 percent accuracy after the aerosol contribution has been subtracted.

The large oscillations in the direct inversion results can be suppressed using the smoothing scheme as described by equation (19). Inversions were performed for the same irradiance profiles using the smoothing scheme with a second-difference constraint on the solutions. The smoothing parameter γ used in the inversions is inversely proportional to the logarithm of the effective transmission T. The reason for choosing a nonlinear variable γ can be seen by referring to equation (14). The measurements g_i are related to the effective tranmission T_i as

$$g_i = \ln (T_i) \tag{31}$$

Irradiance errors in the measurements can be included in the quantities g_i as

$$g_i = \ln (H_i + \Delta H_i)/H_o \tag{32}$$

where ΔH_i are the errors associated with the irradiance measurements H_i, and H_o is the unattenuated irradiance. For ΔH_i to be small compared to H_i and H_o, we can expand equation (32) and obtain

$$g_i = \ln(H_i/H_o) + \Delta H_i/H_i \tag{33}$$

The first term on the right side of equation (33) is the signal term, while the second term is the noise term. In choosing the γ

to be inversely proportional to the signal to noise ratio, we then arrive at the particular form of γ as discussed above.

Figures 13 through 16 show the inversion results with the smoothing scheme. Considerable improvement in the solutions has been obtained with the fine structure oscillations being suppressed. Aerosol extinction profiles can be reproduced to better than 10 percent accuracy, while ozone extinction profiles can be reproduced to better than 5 percent.

Other models for the vertical distributions of aerosol also have been used in simulating the four channels irradiance profiles for inversion. Figures 17 through 19 illustrate the inversion results from the smoothing scheme for the three aerosol channels based on Fenn's background aerosol model (ref. 2), while figures 20 through 22 illustrate inversion results for a moderate volcanic aerosol distribution (ref. 2). The noise levels in these figures are relative to the full scale irradiance levels. The accuracies of the inverted results for different aerosol distributions are generally similar.

CONCLUSIONS

In this study we have examined the retrieval of the vertical distributions of stratospheric aerosol and ozone from multi-wavelength measurements of transmitted radiation in the solar occultation experiment. Inversions of simulated irradiance profiles computed from different aerosol and ozone vertical distributions have been performed at 0.38, 0.45, 0.6, and 1.0 μm wavelengths. The inversion results indicated that aerosol extinction profiles can be retrieved to an accuracy of better than 10 percent over most of the stratosphere, while ozone vertical distribution can be retrieved to better than 5 percent accuracy.

The accuracy of the inversion techniques as discussed in this study is not dependent on the method of measurements. Irradiance data can be obtained either with the radiometer pointing to a fixed location on the solar image during the occultation event or with the radiometer scanning across the solar image. Provided that the irradiance errors associated with each measurement are within the same level, accuracy of the retreived profiles will be similar.

This study has been concerned mainly with the retrieval of multi-wavelength extinction profiles for the stratospheric constituents. Since different wavelength extinction coefficients of the stratospheric aerosol can be measured at each altitude, these wavelength-dependent extinction coefficients can be used to retrieve some physical properties of the stratospheric aerosol such as size distribution, number density, and index of refraction. A future study to evaluate this problem will be very important.

REFERENCES

1. T.J. Pepin, Ph.D. thesis, University of Minnesota (1970).
2. R.W. Fenn, unpublished works.
3. L. Elterman, AFCRL-68-0153 (1968).
4. J. Fontanella, A. Girard, L. Gramont, and N. Louisnard, Applied Optics, 14, 825 (1975).
5. M. Born, and E. Wolf, Principles of Optics, Pergamon Press, Oxford, 1964, p. 123.
6. P.N. Tverskoi, Physics of the Atmosphere, Israel Program for Scientific Translations, p. 457 (1965).
7. S. Twomey, J. Assn. Computing Machinery, 10, 99 (1963).
8. D.L. Phillips, J. Assn. Computing Machinery, 9, 97 (1962).
9. B.J. Conrath, and I. Revah, NASA TM X-62, 150 (1972).
10. W.L. Smith, Applied Optics, 9, 1993 (1970).

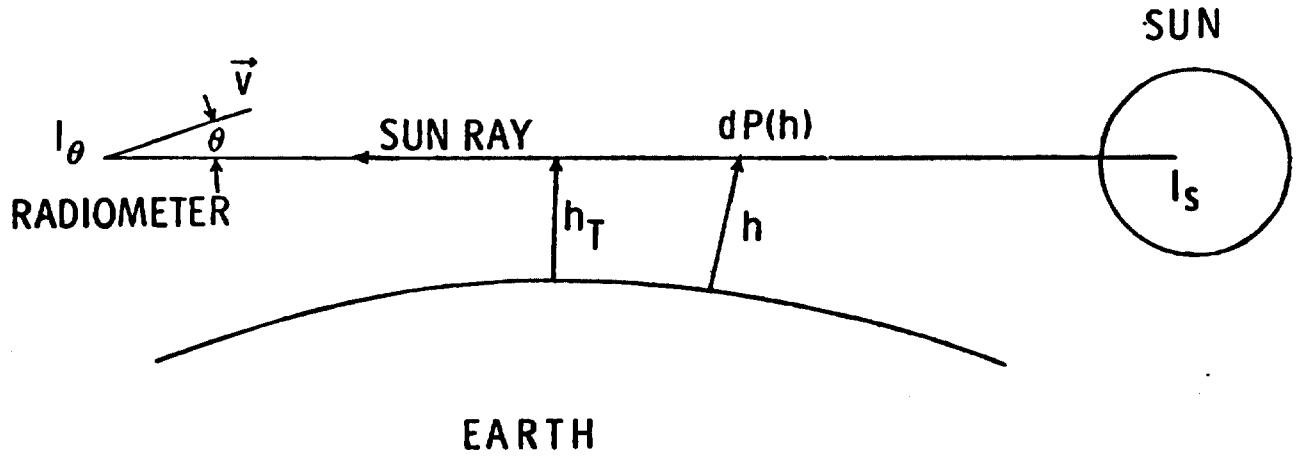

Figure 1. Solar occultation geometry.

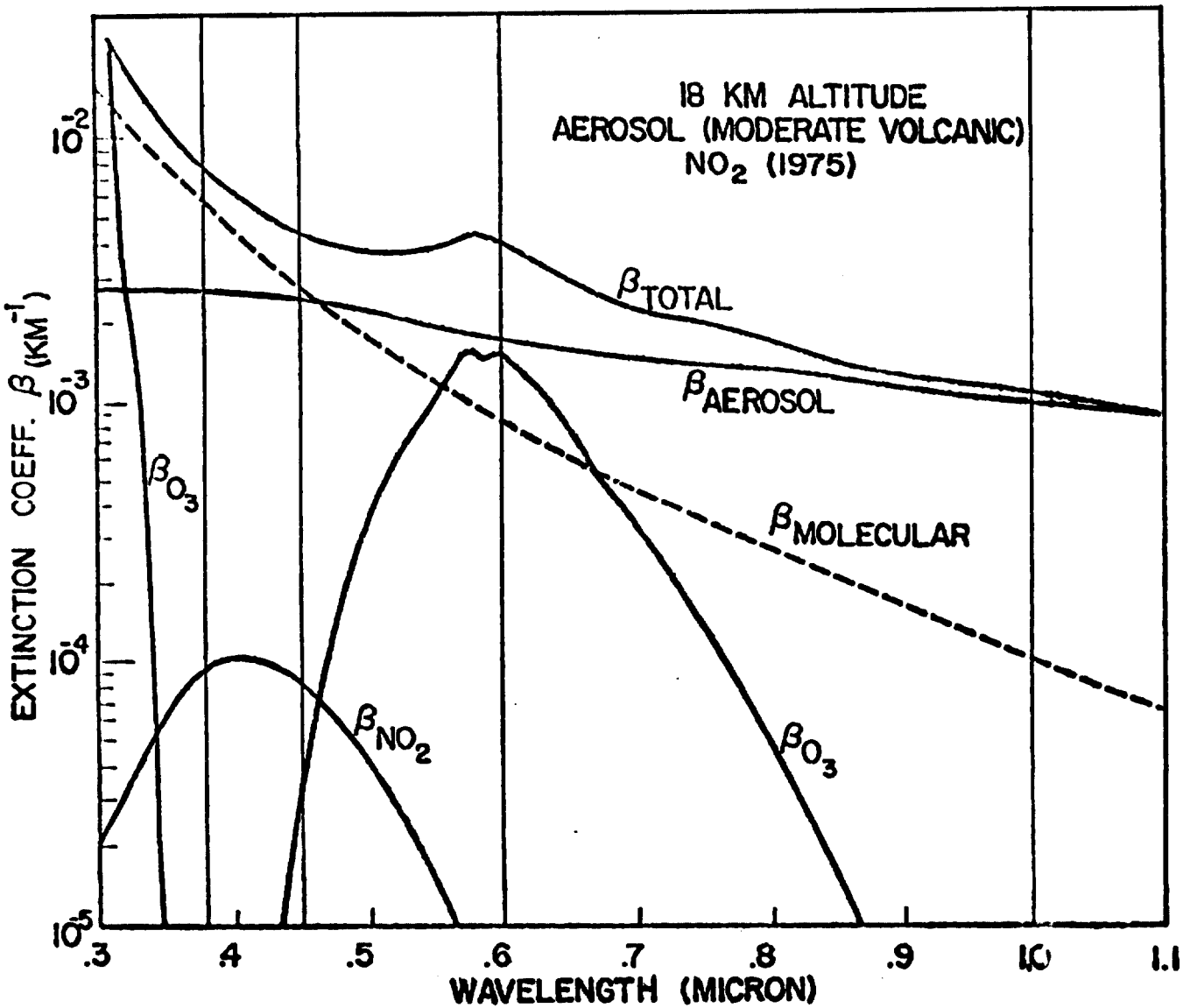

Figure 2. Extinction coefficients model as a function of wavelength at an altitude of 18 km.

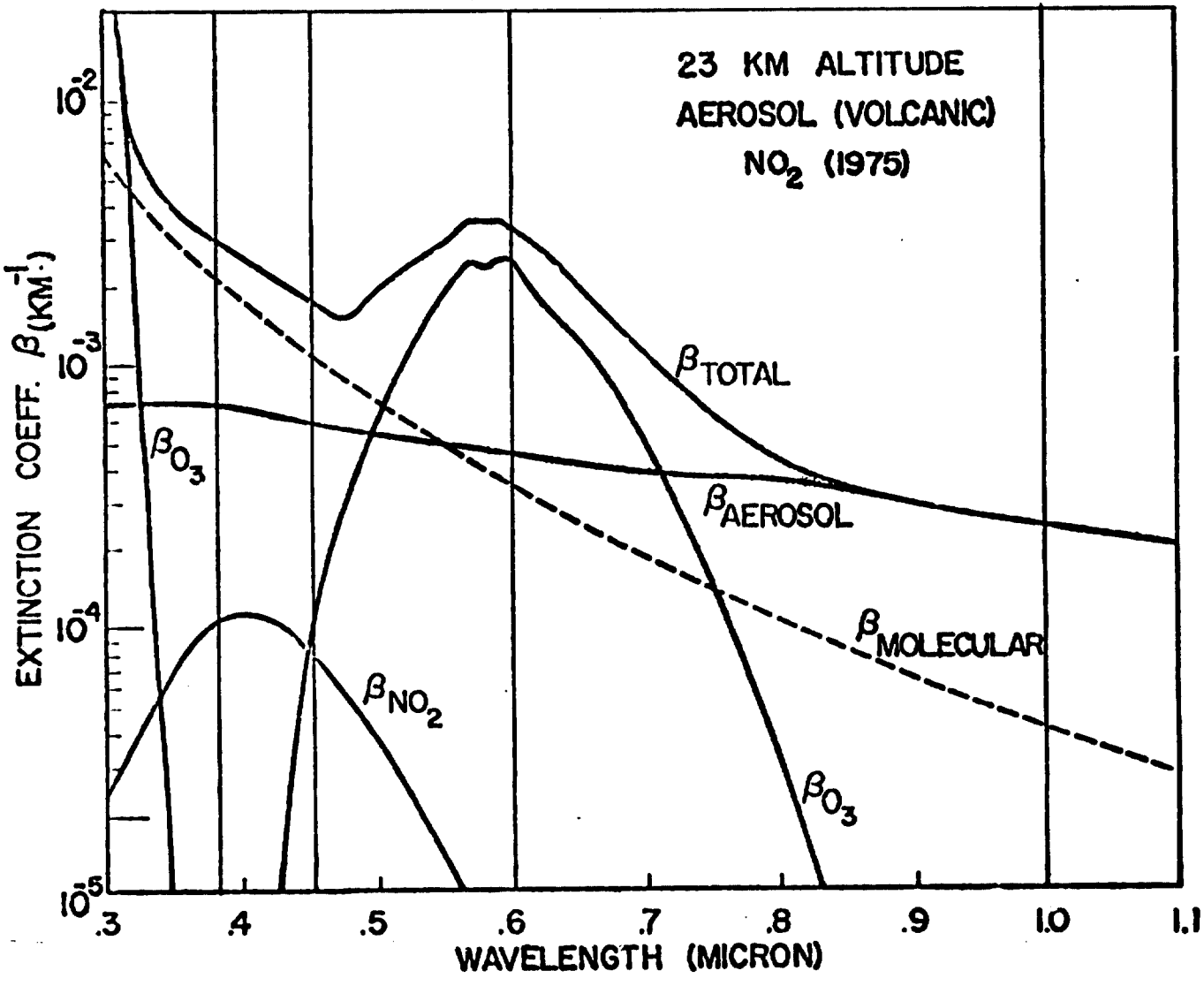

Figure 3. Extinction coefficients model as a function of wavelength at an altitude of 23 km.

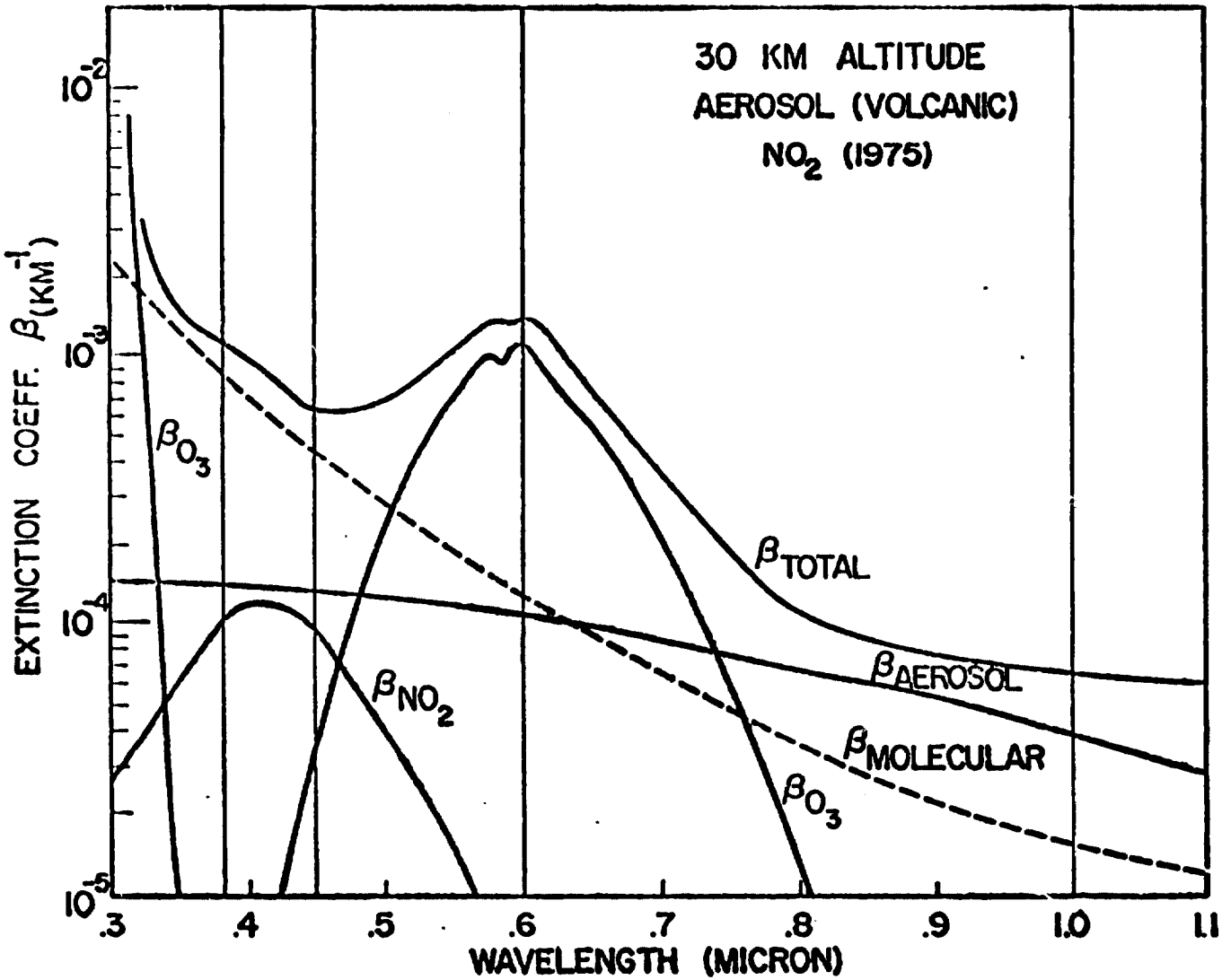

Figure 4. Extinction coefficients model as a function of wavelength at an altitude of 30 km.

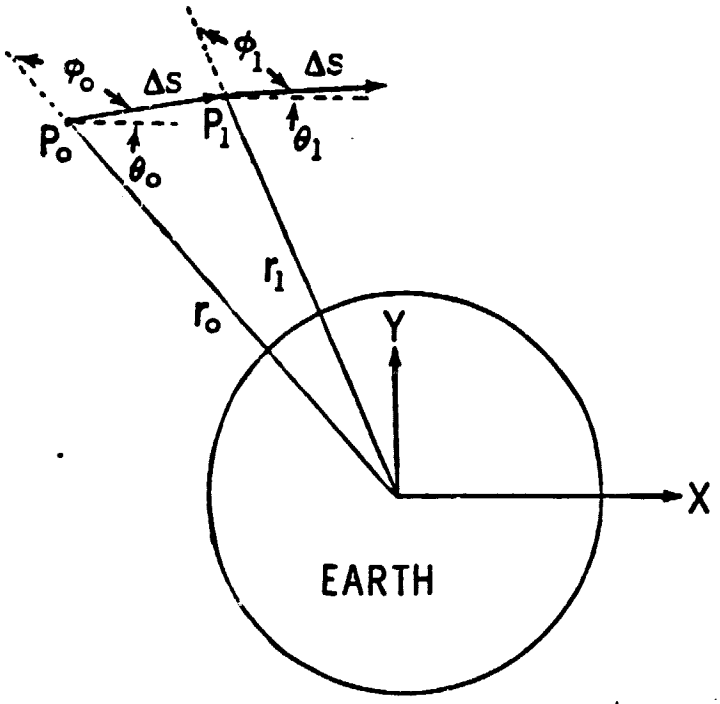

Figure 5. Ray tracing geometry for atmospheric refraction calculations.

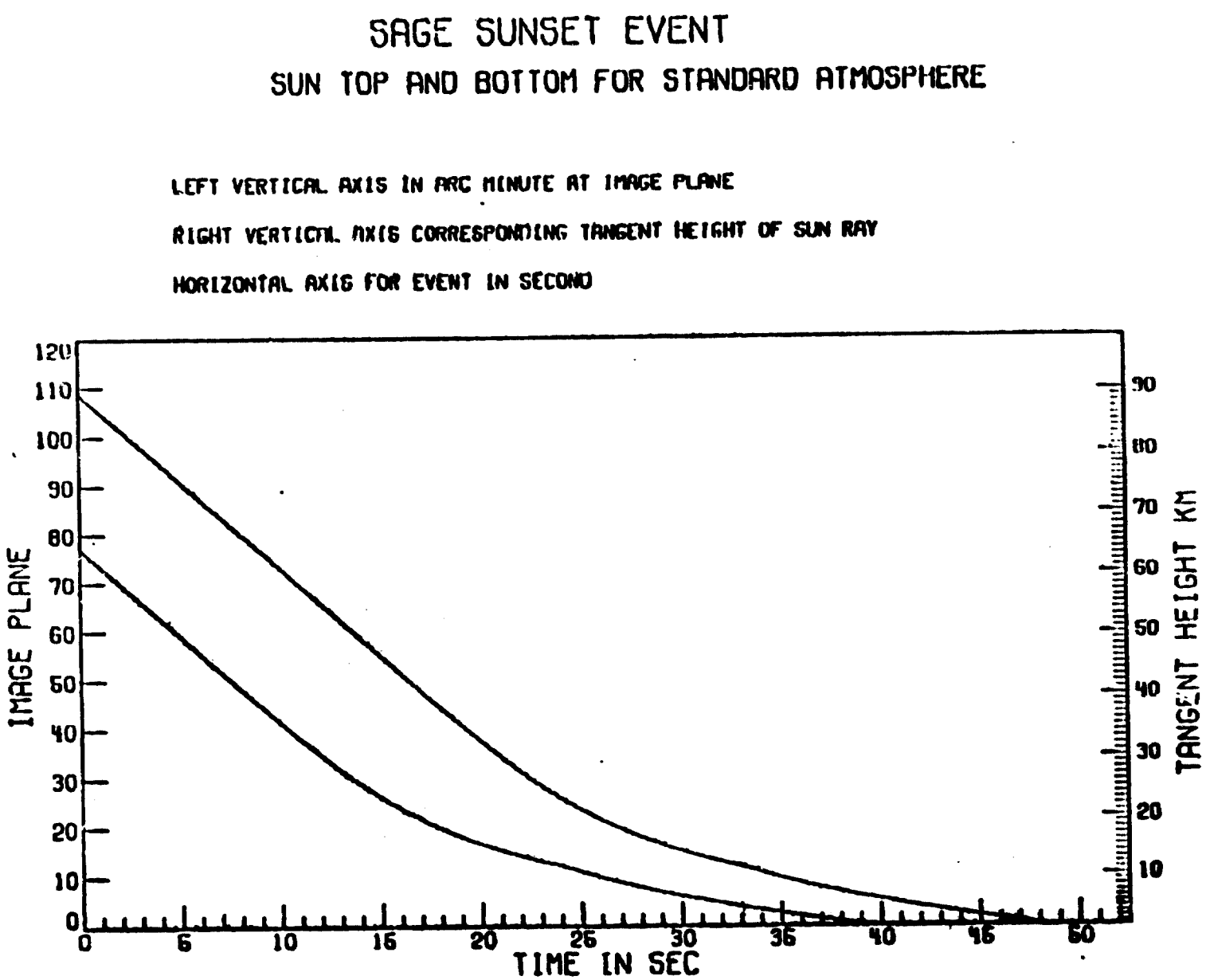

Figure 6. The vertical extent of the solar image during a sunset event from the refraction calculations.

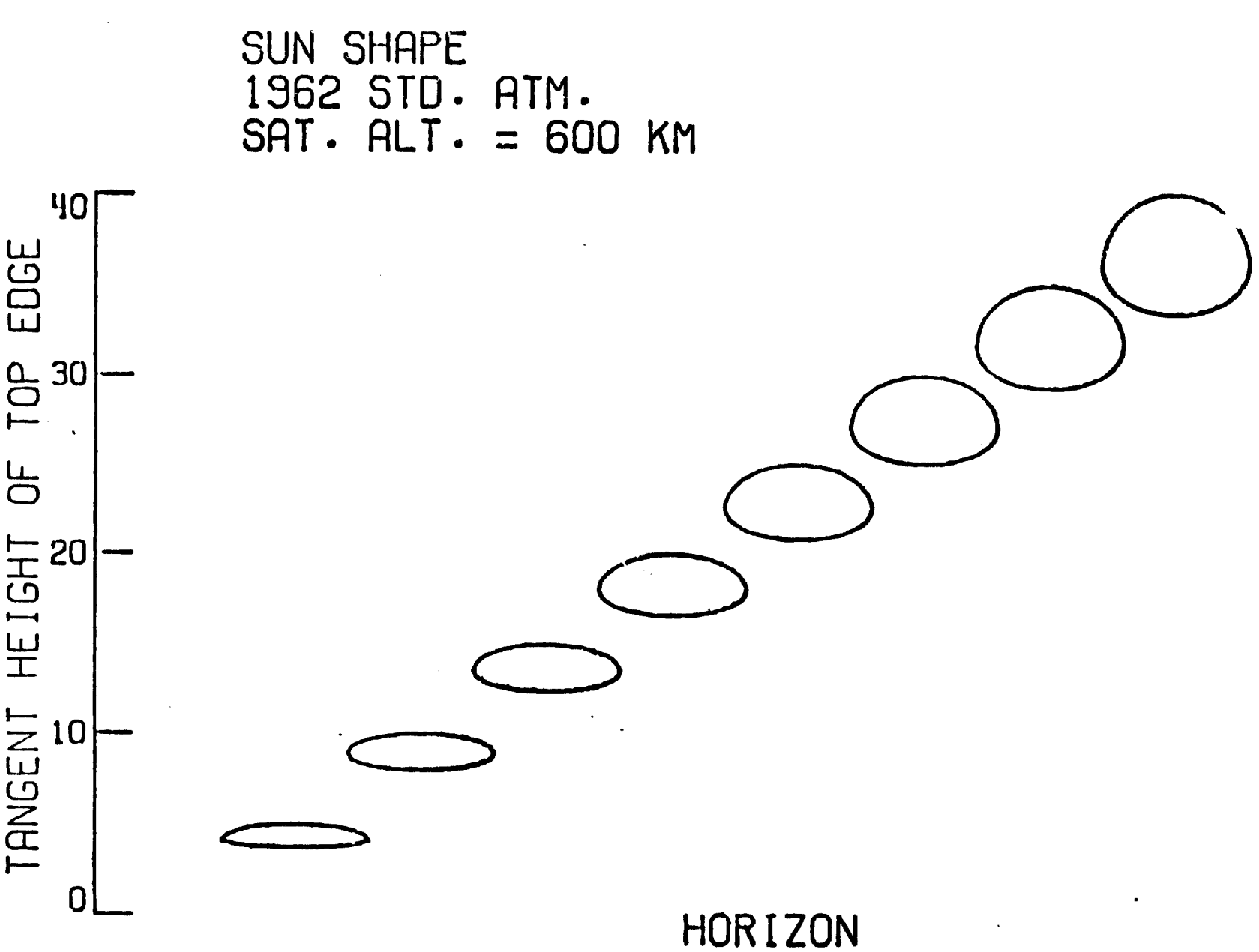

Figure 7. Sun shape images as observed on the spacecraft for different apparent altitudes from the refraction calculations.

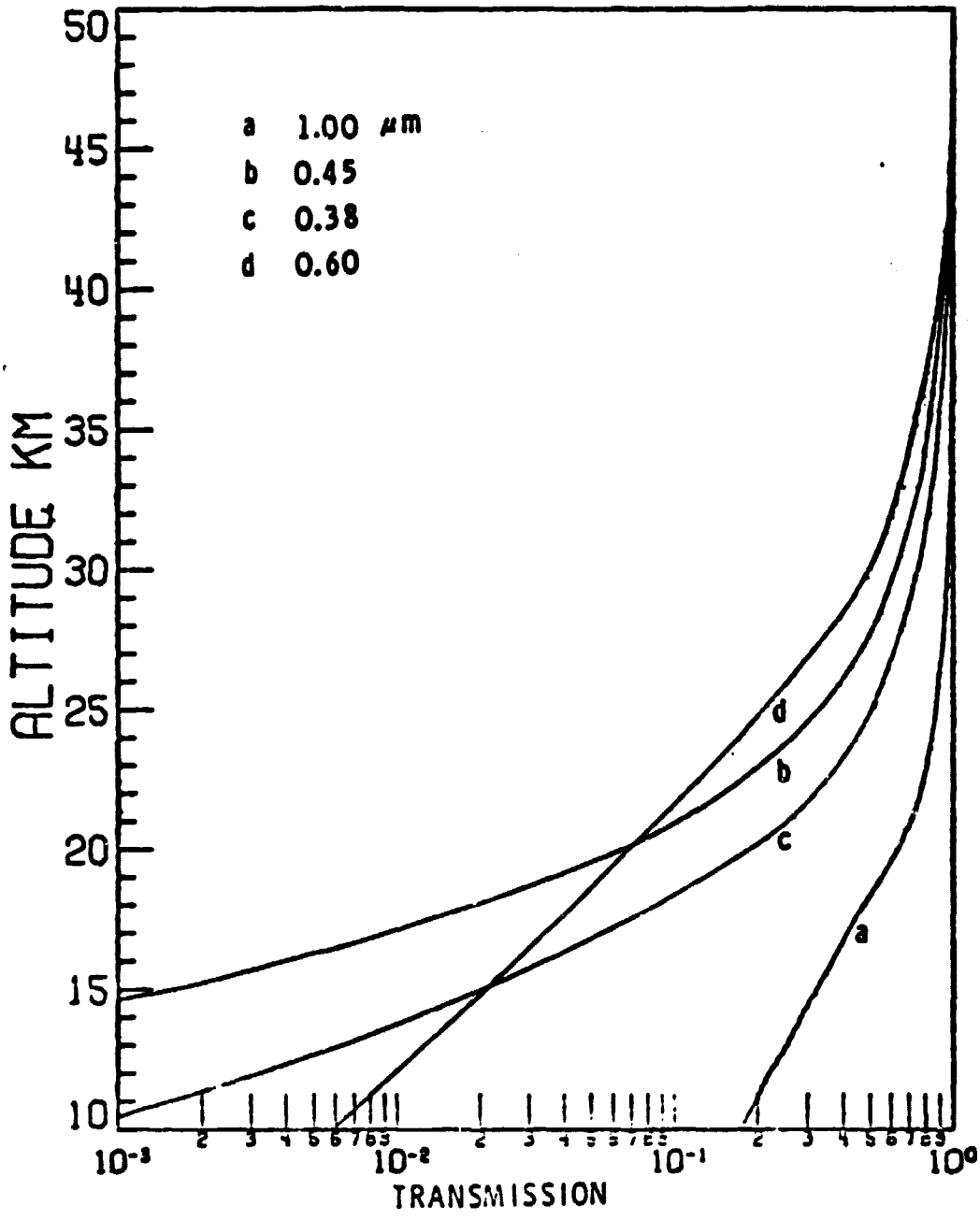

Figure 8. Atmospheric transmission versus altitude for the four wavelengths 0.38, 0.45, 0.6, and 1.0 micron.

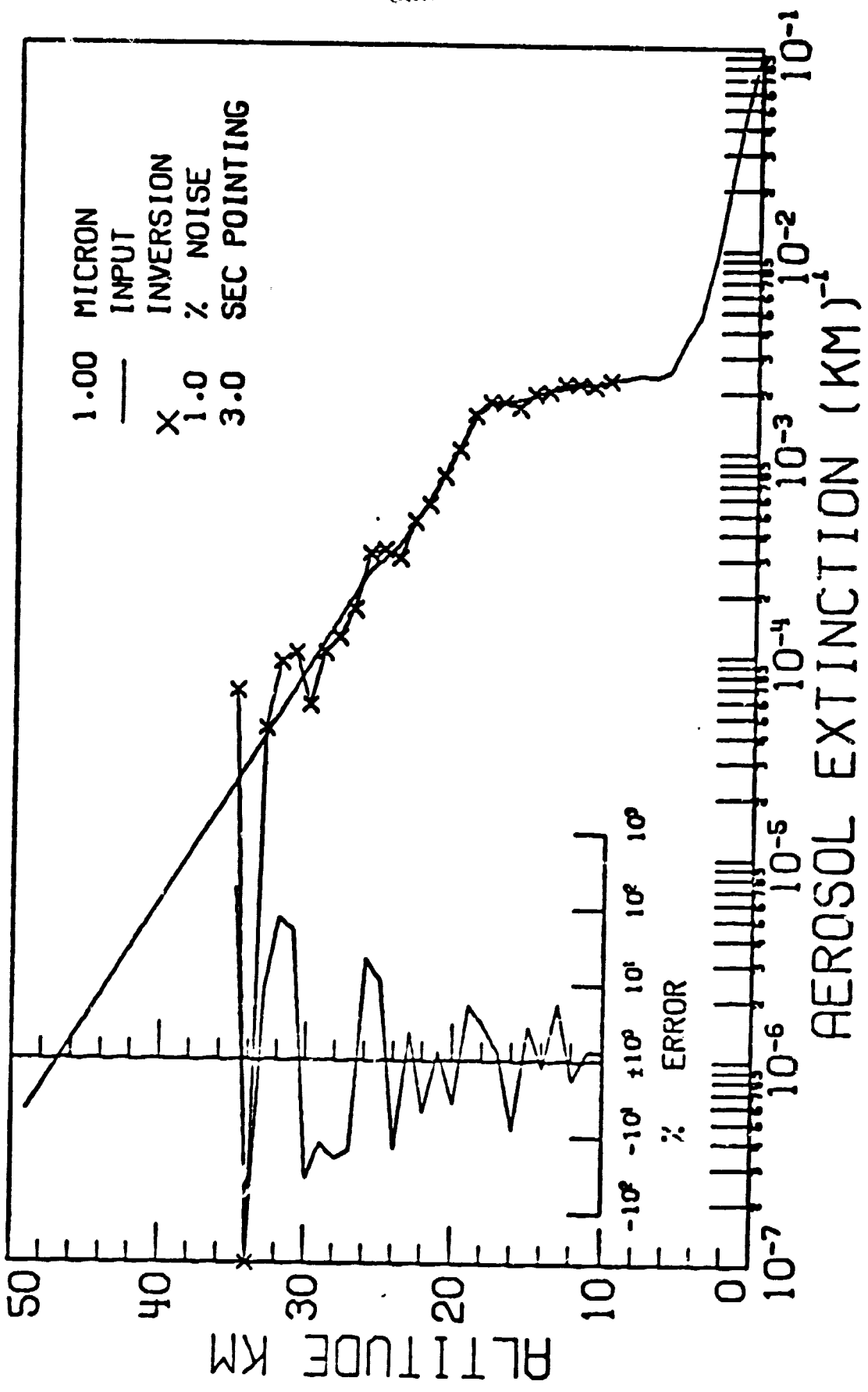

Figure 9. Direct inversion results from simulated irradiance profile at 1.0 micron wavelength.

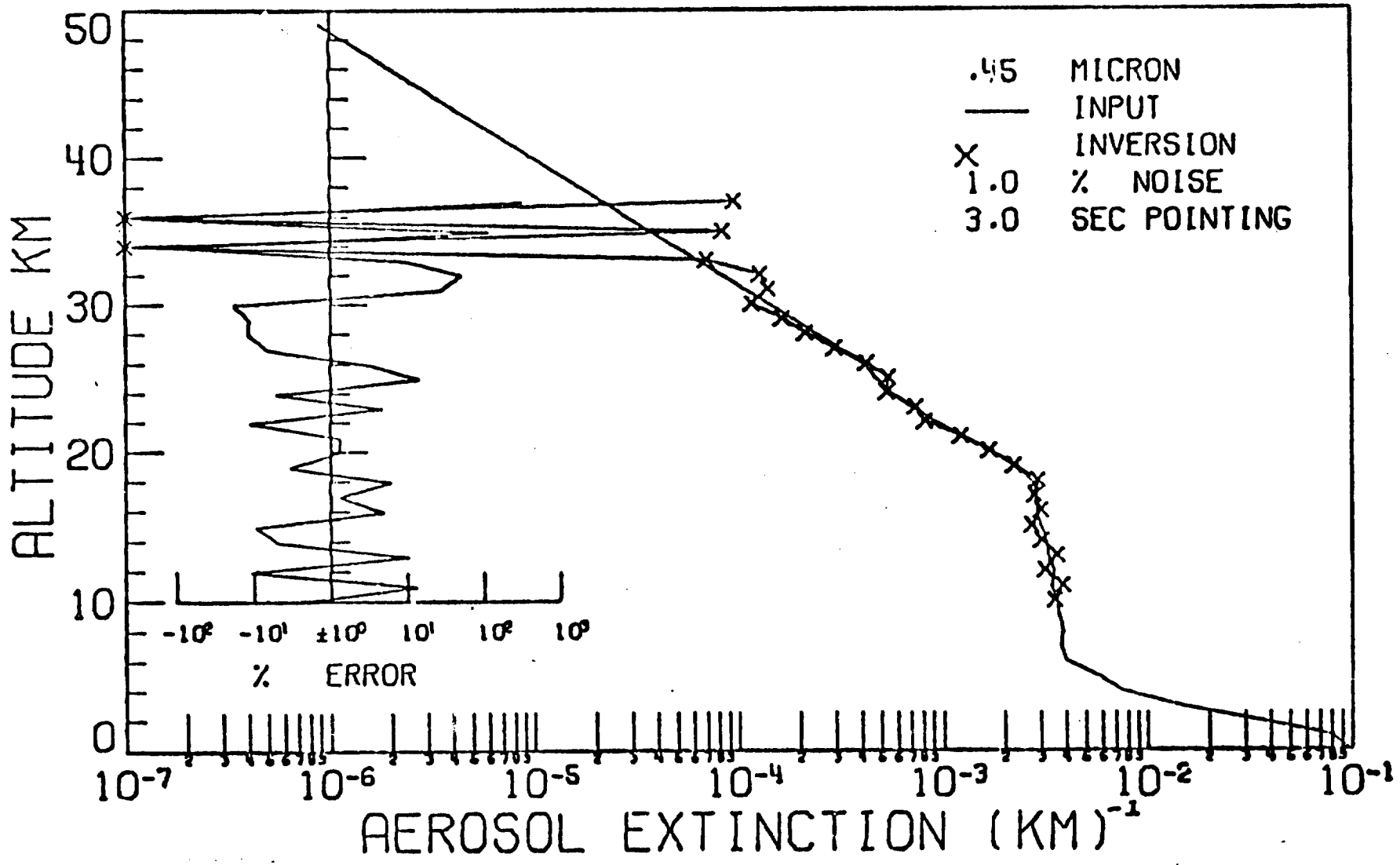

Figure 10. Direct inversion results from simulated irradiance profile at 0.45 micron wavelength.

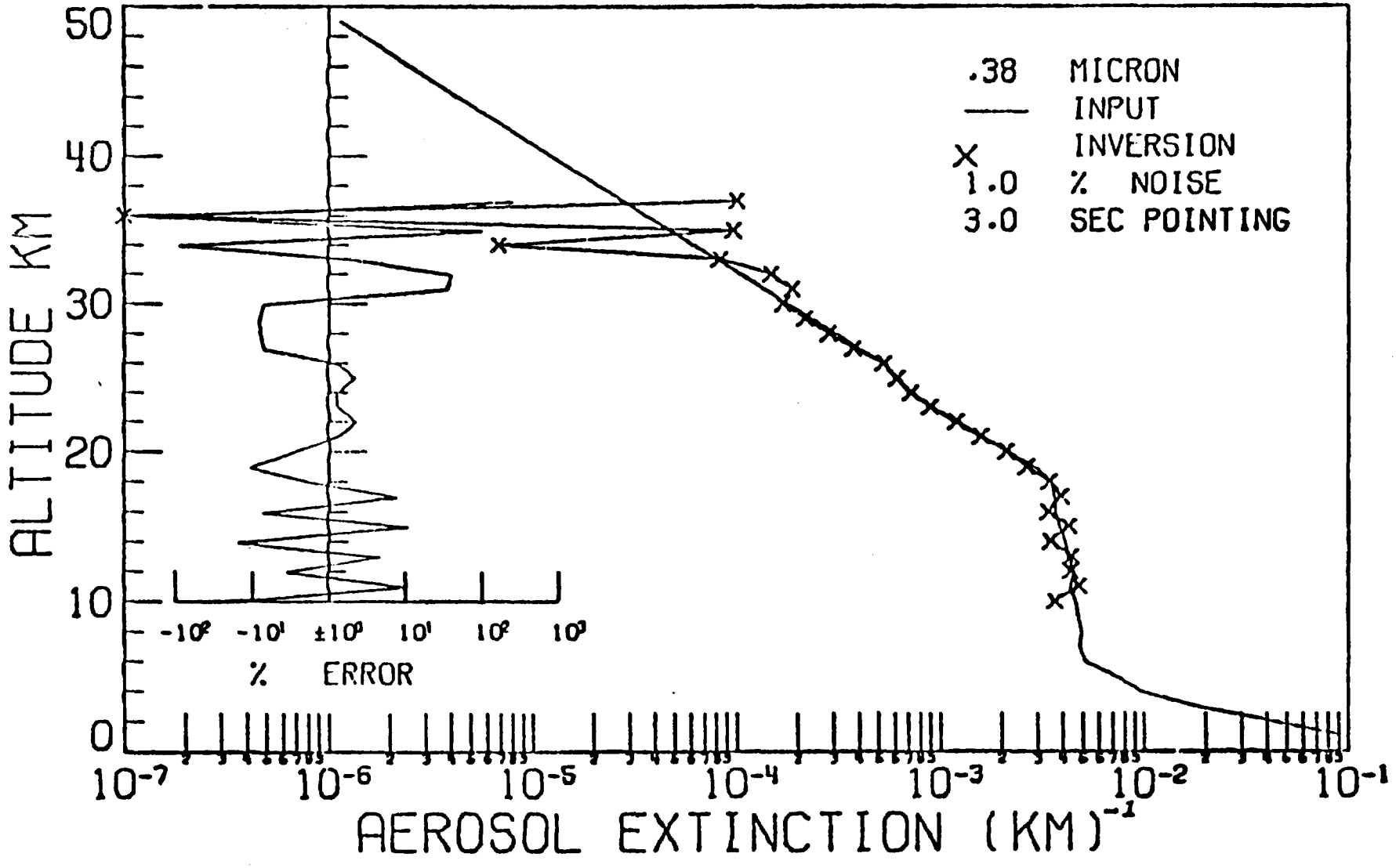

Figure 11. Direct inversion results from simulated irradiance profile at 0.38 micron wavelength.

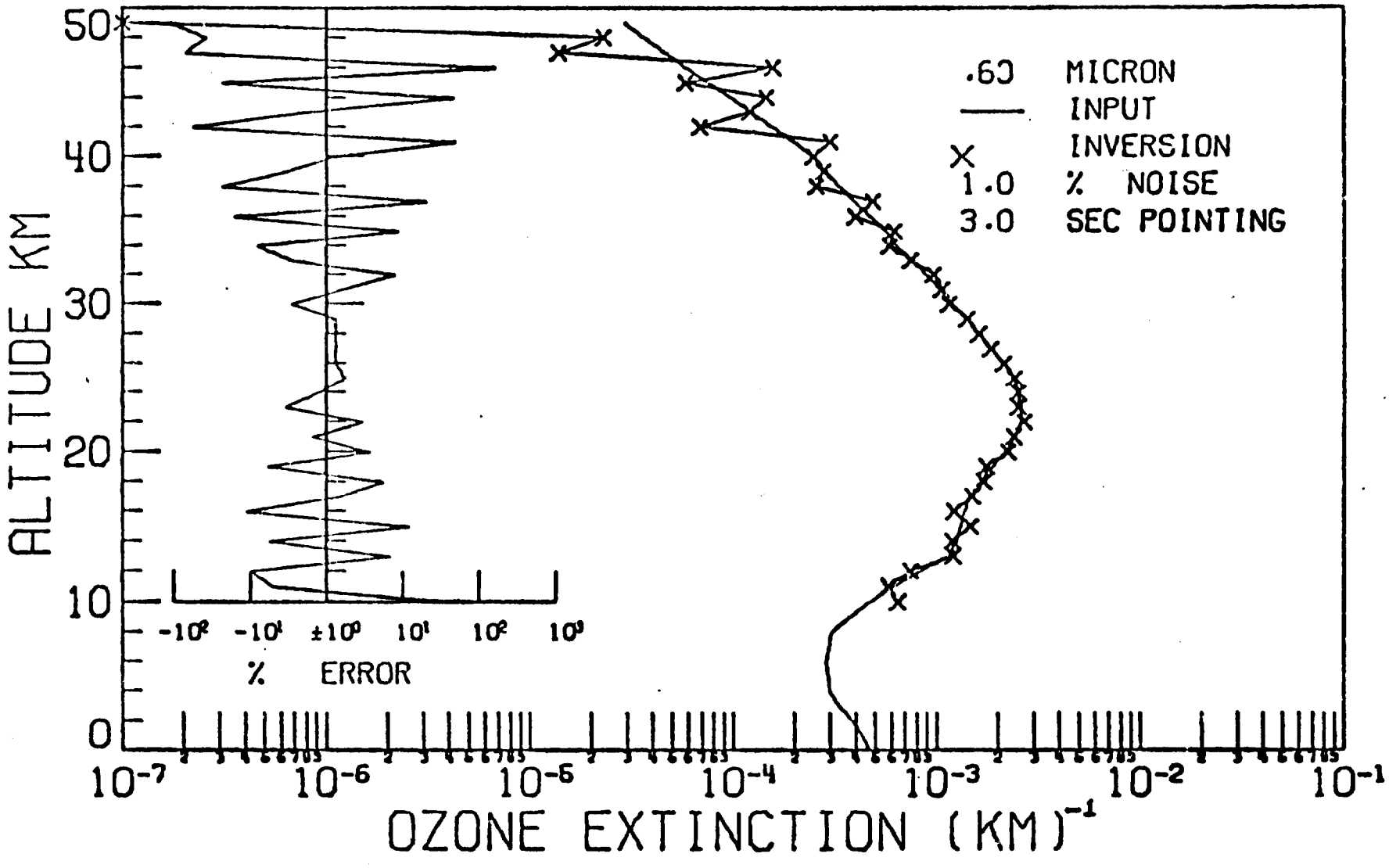

Figure 12. Direct inversion results from simulated irradiance profile at 0.6 micron wavelength for ozone.

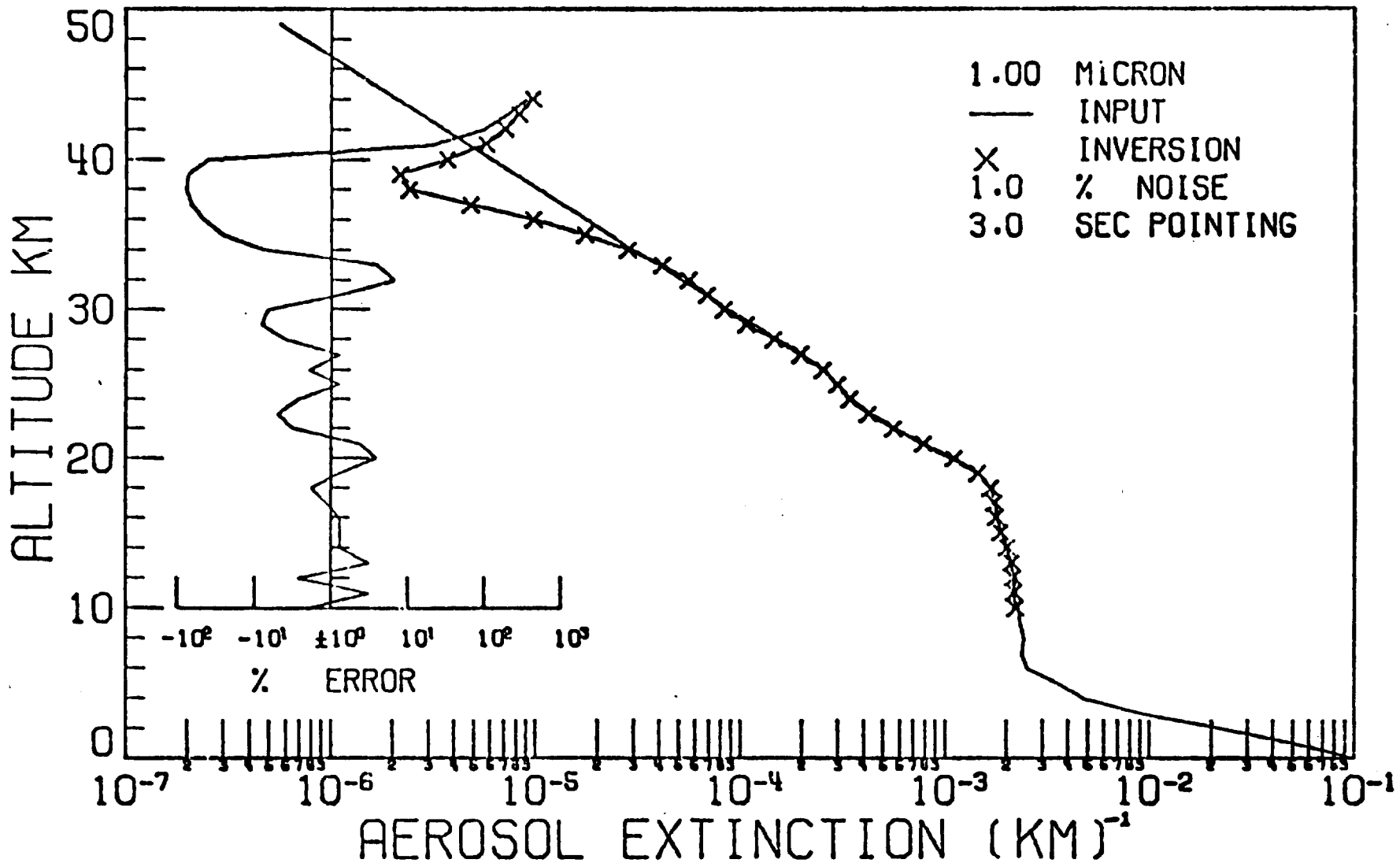

Figure 13. Inversion results with smoothing at 1.0 micron.

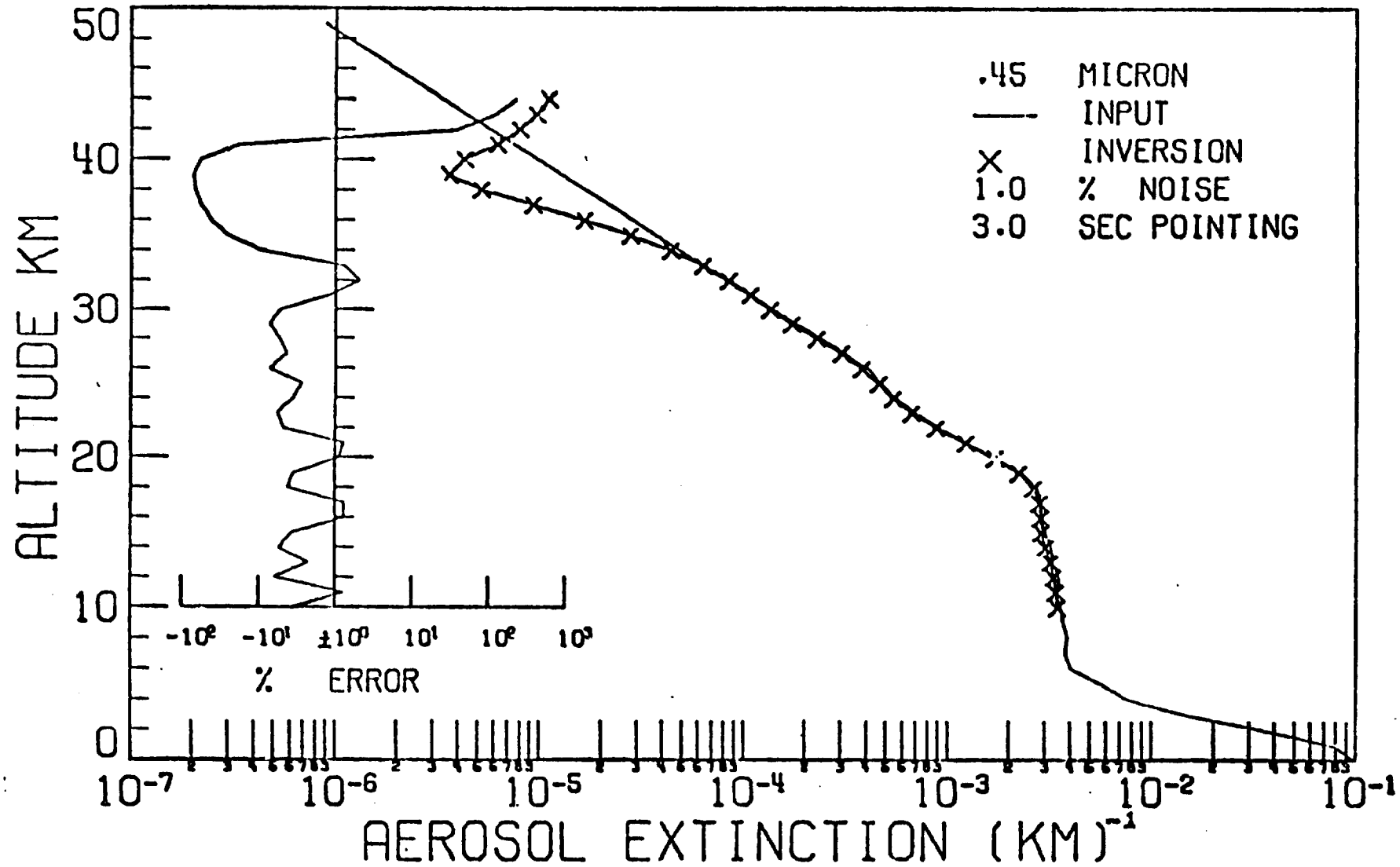

Figure 14. Inversion results with smoothing at 0.45 micron.

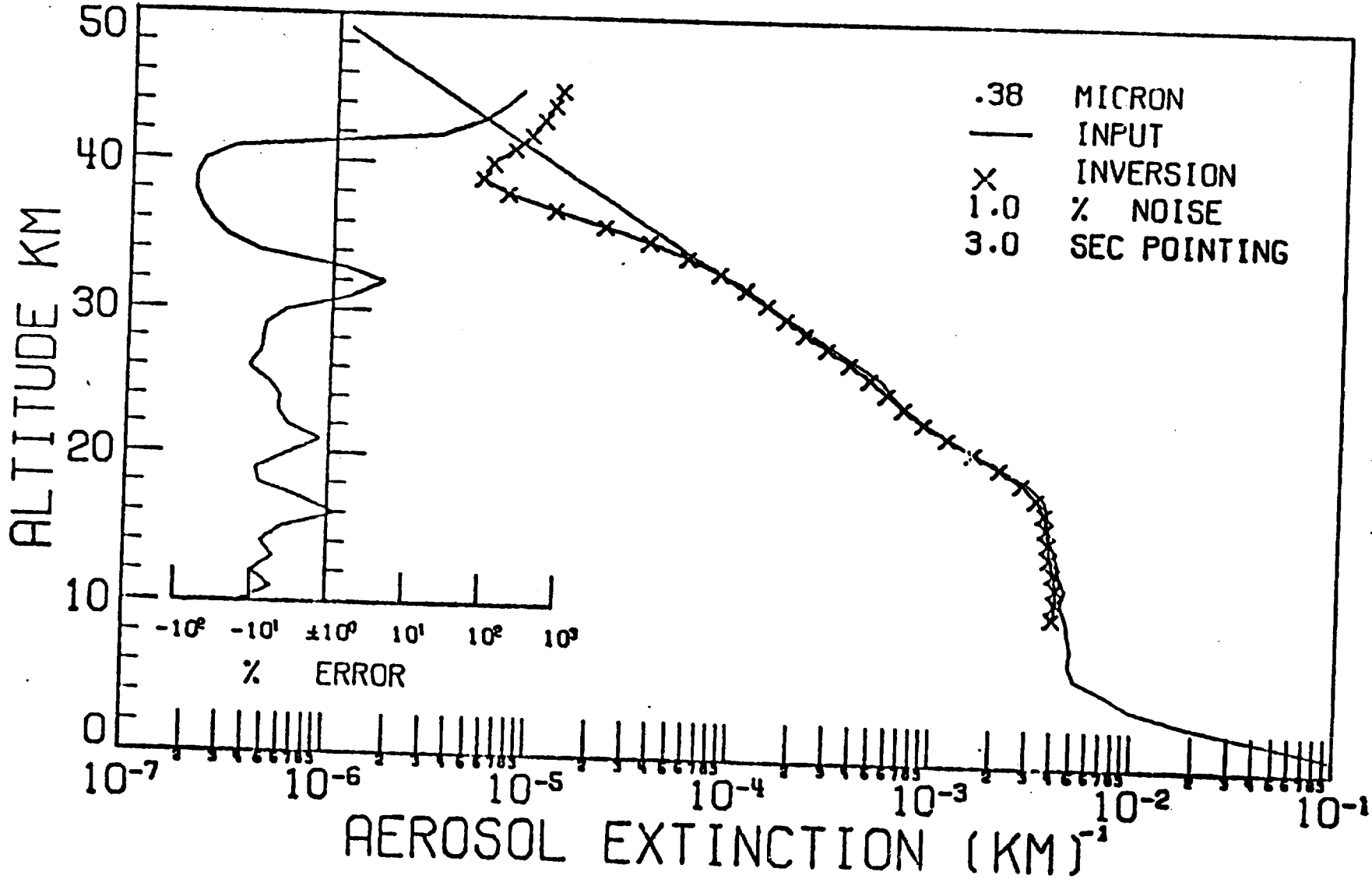

Figure 15. Inversion results with smoothing at 0.38 micron.

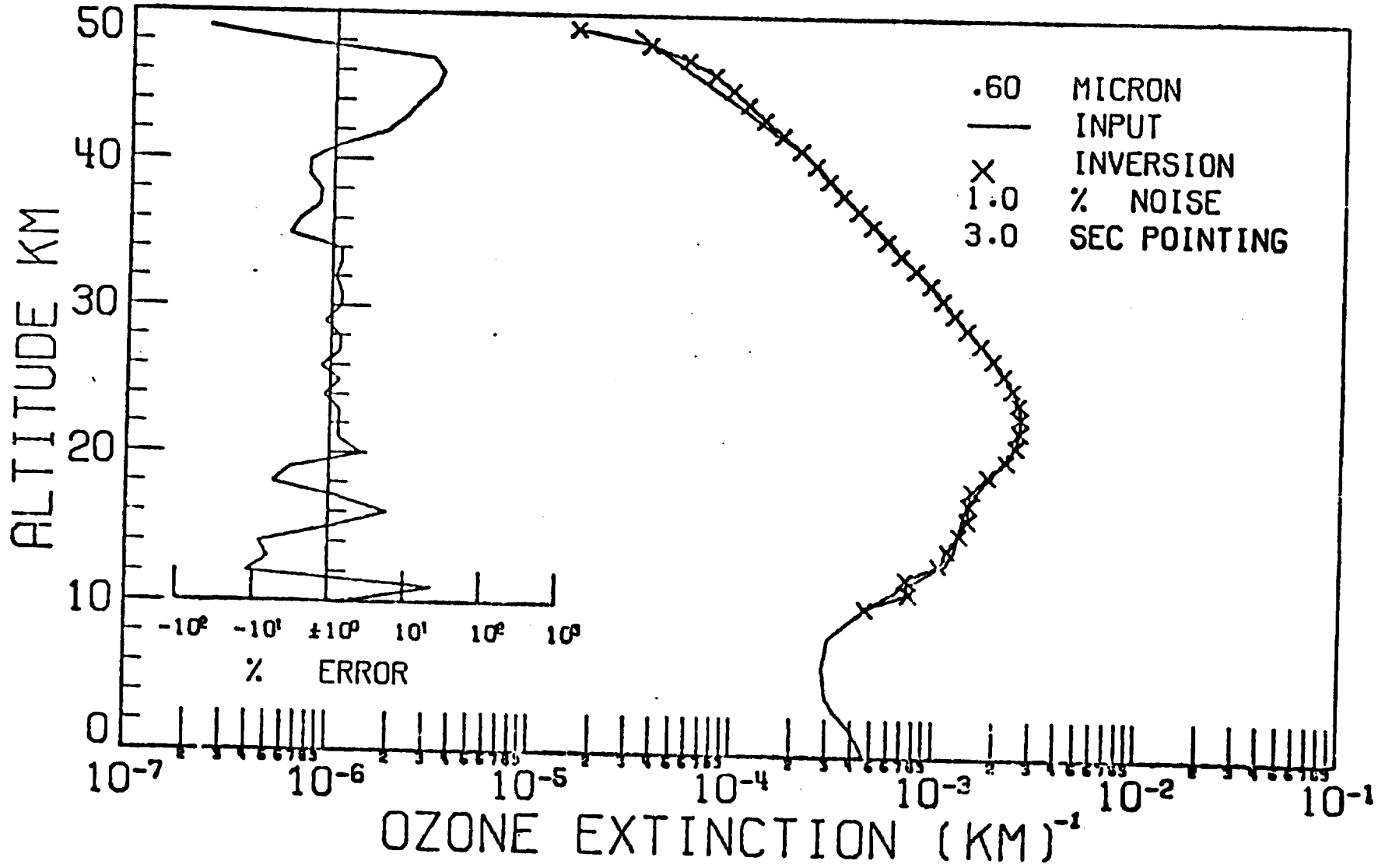

Figure 16. Inversion results with smoothing at 0.6 micron for ozone.

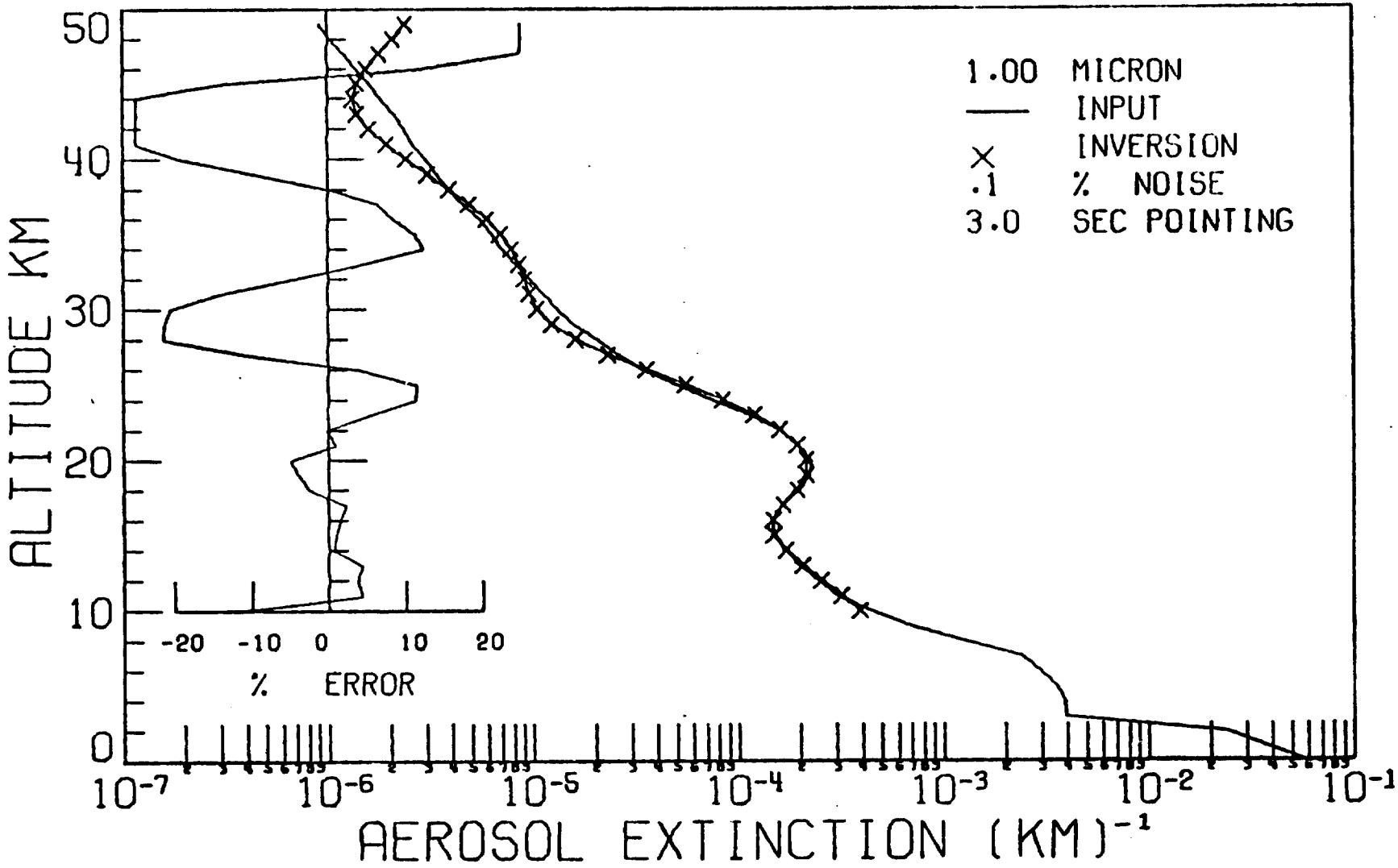

Figure 17. Inversion results with smoothing at 1.0 micron for a background aerosol model.

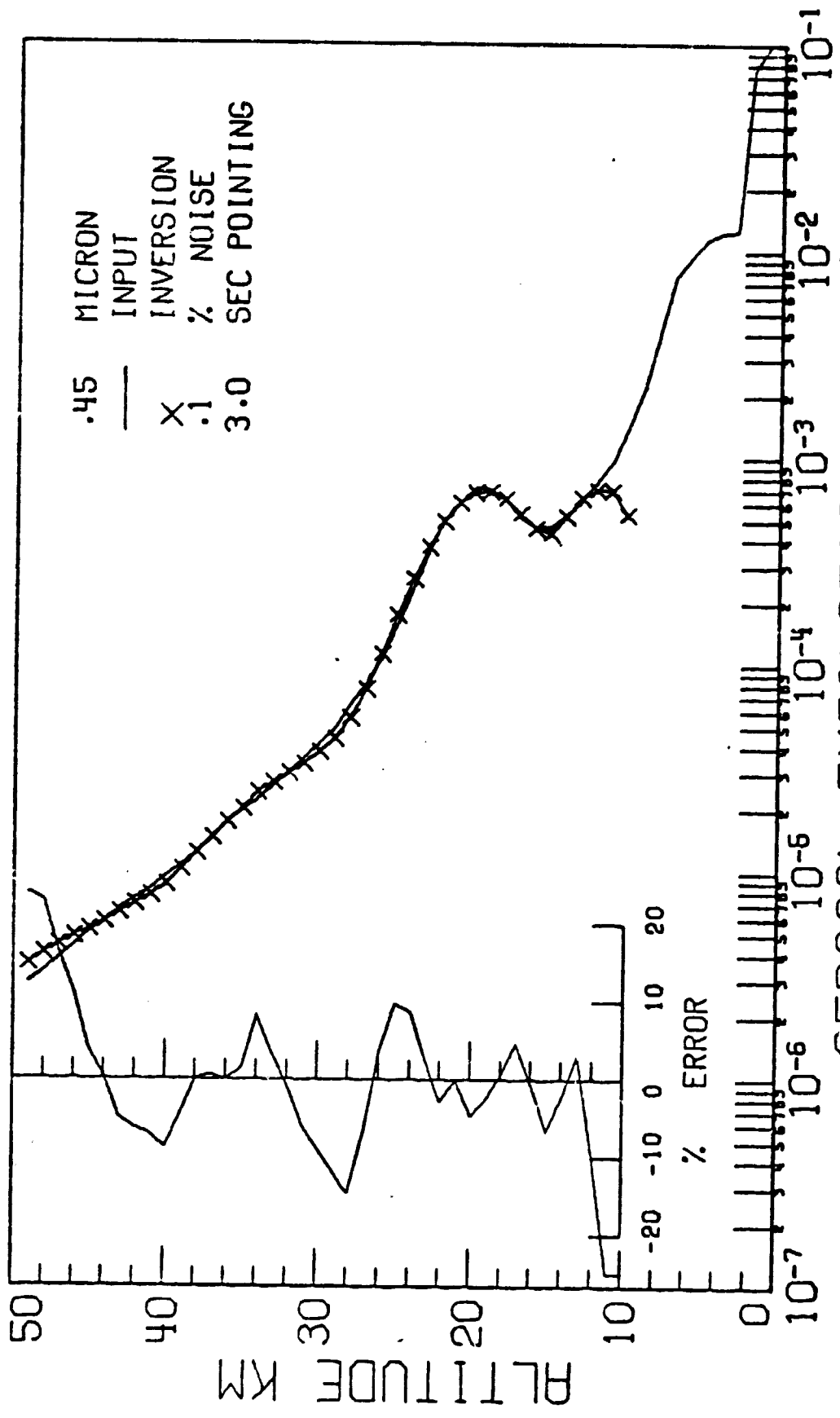

Figure 18. Inversion results with smoothing at 0.45 micron for a background aerosol model.

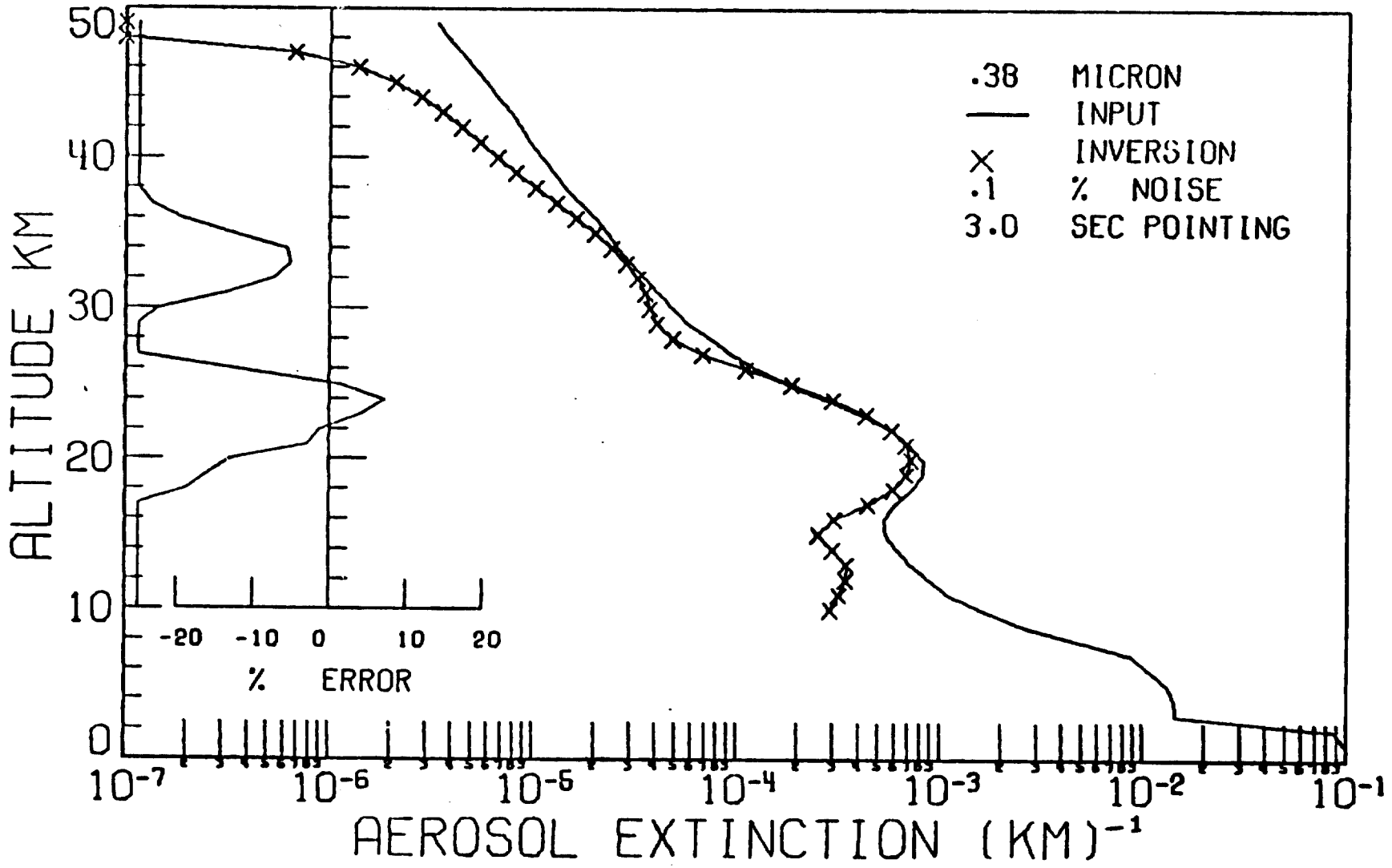

Figure 19. Inversion results with smoothing at 0.38 micron for a background aerosol model.

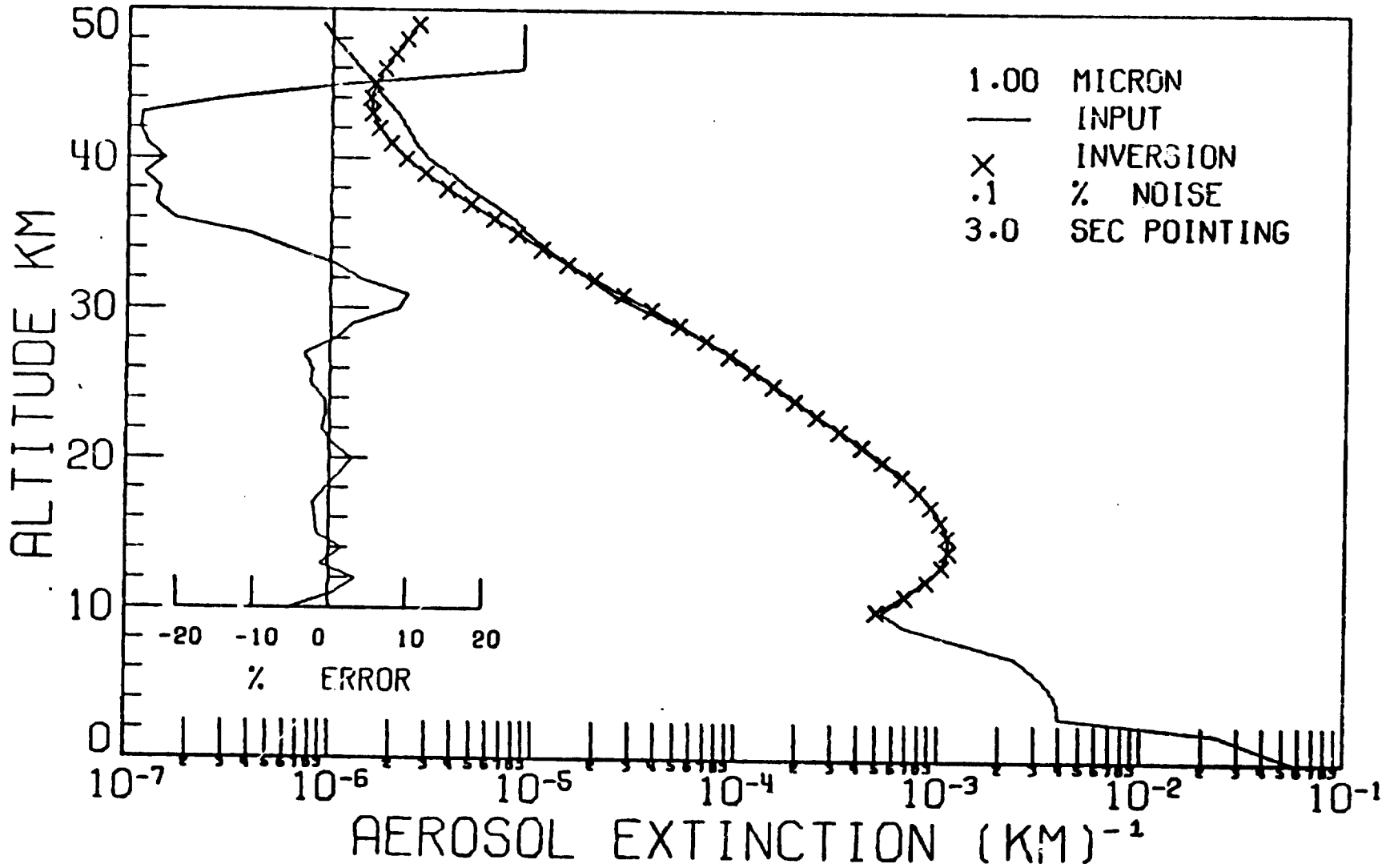

Figure 20. Inversion results with smoothing at 1.0 micron for a moderate volcanic aerosol model.

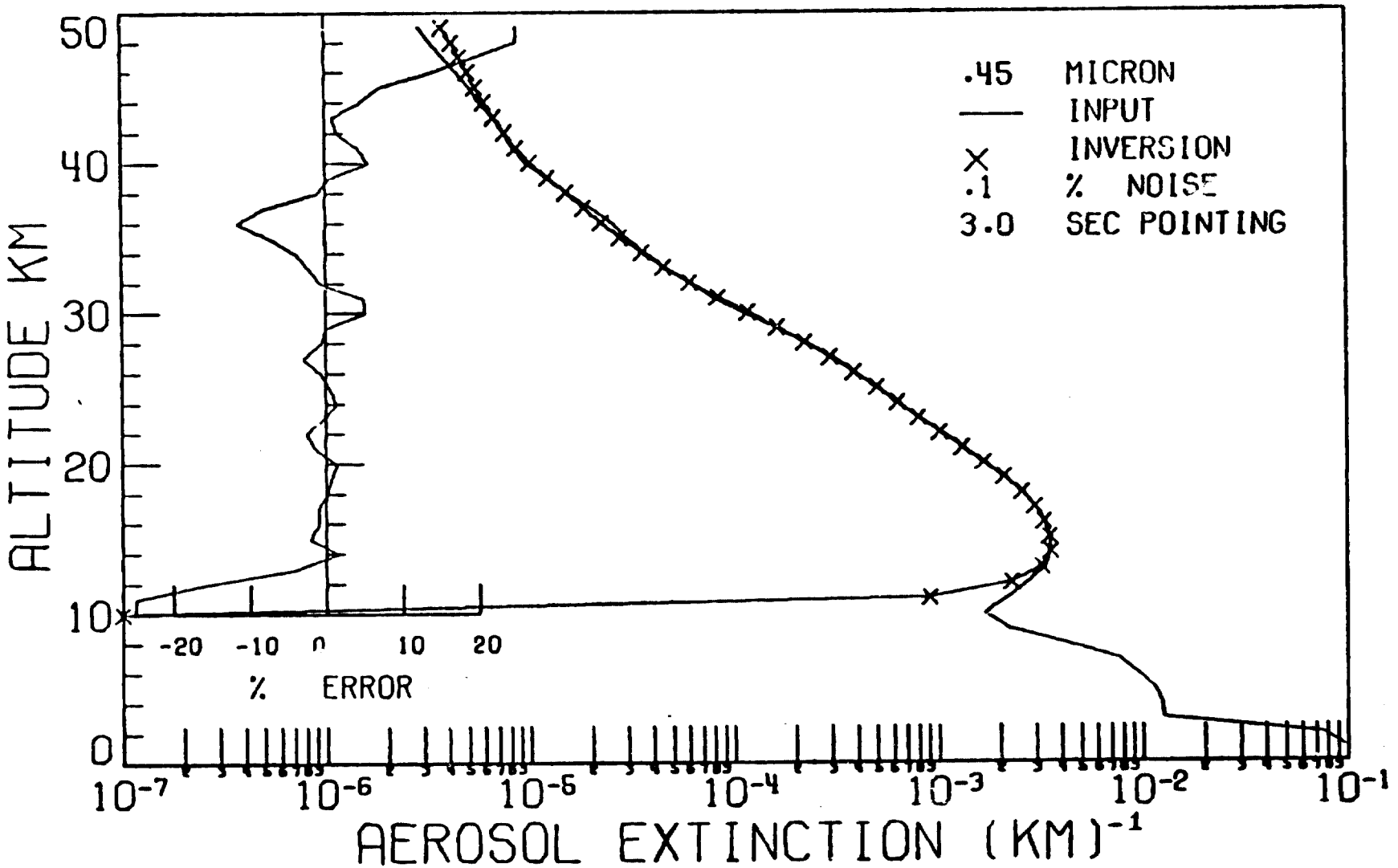

Figure 21. **Inversion results with smoothing at 0.45 micron for a moderate volcanic aerosol model.**

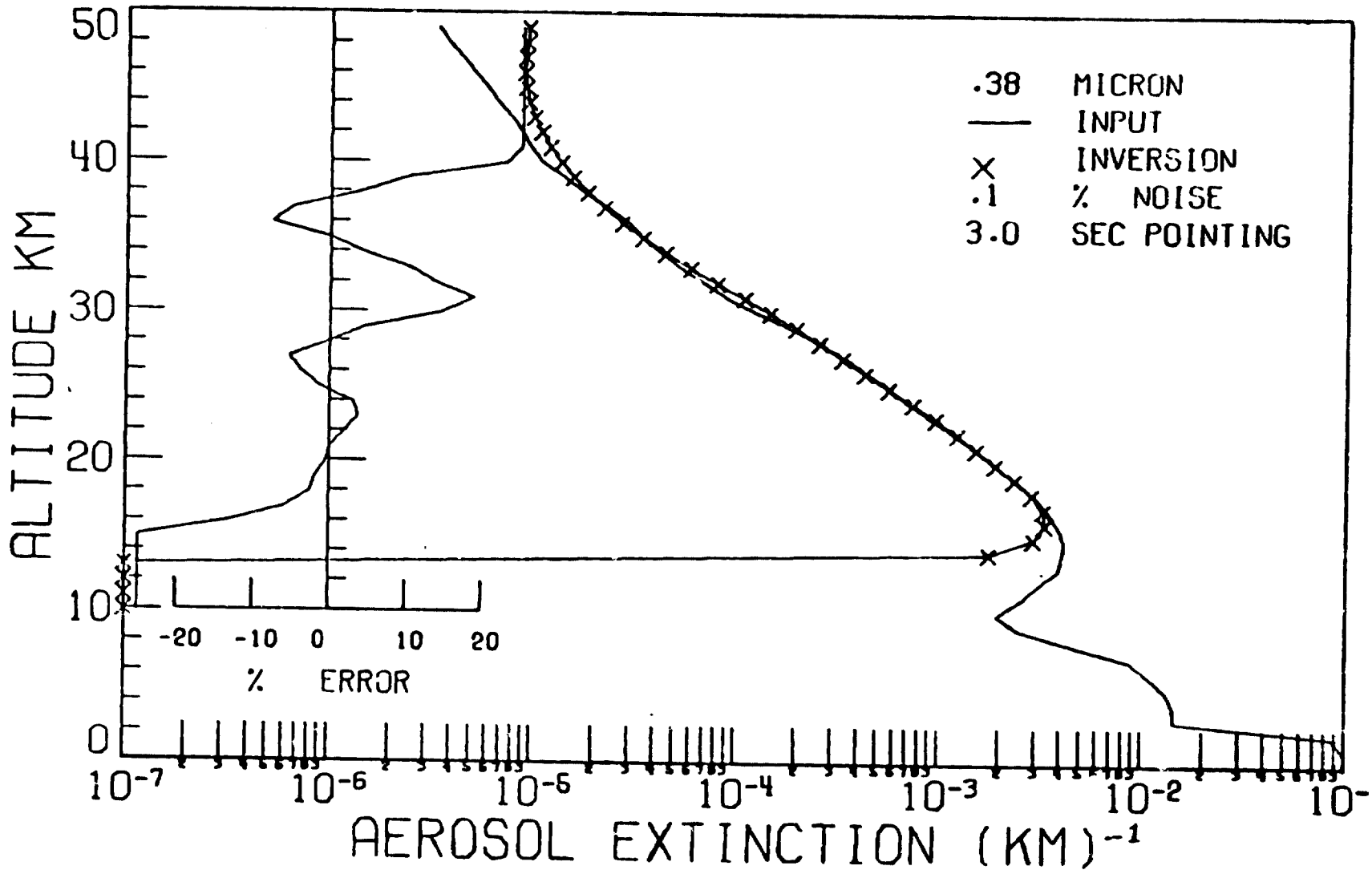

Figure 22. Inversion results with smoothing at 0.38 micron for a moderate volcanic aerosol model.